Periodic Analysis of a 2-D Negative Refractive Index Transmission Line Structure

Anthony Grbic, *Student Member, IEEE,* and George V. Eleftheriades, *Senior Member, IEEE*

***Abstract*—The propagation characteristics of a two-dimensional (2-D) negative refractive index (NRI) transmission line (TL) structure are explained using Bloch theory. Bloch analysis of a generalized 2-D periodic electrical network is performed and the results are applied to the NRI TL structure. A 2-D Brillouin diagram of the NRI TL metamaterial is presented and its band structure is intuitively explained. Voltage and current relationships, Bloch impedance expressions and dispersion equations which aid in the design, proper excitation and termination of such structures are derived. Effective material parameters for regions of isotropic and homogeneous operation are also derived, providing a simplified understanding of the NRI TL metamaterial's 2-D band structure. Finally, simulations of negative refraction for a relative refractive index of $n = -1$ are shown. The simulation results verify the analytic expressions presented in this paper and demonstrate the proper termination and excitation of finite size structures.**

***Index Terms*—Left-handed media, loaded transmission lines, metamaterials, negative refractive index, periodic structures, printed circuits.**

I. Introduction

COMPOSITE materials exhibiting simultaneously negative values of permittivity and permeability have attracted widespread interest in the past few years [1]–[4]. The first structure exhibiting such properties combined an array of metallic wires to attain negative permittivity and an array of split-ring resonators to achieve negative permeability [4]. The structure exhibited backward-wave (BW) propagation characteristics and was used to demonstrate negative refraction. Its implementation has given rise to a new class of artificial electromagnetic materials (metamaterials) exhibiting exotic properties. In particular, the possible subwavelength resolving properties of such materials [2] have stirred much excitement and renewed interest in electromagnetic phenomena associated with negative refractive index (NRI) materials, first investigated by Veselago in the 1960s [5].

More recently, an *L-C* loaded transmission line (TL) network implemented in a cellular form was also shown to exhibit NRI properties. Fig. 1 depicts the unit cell of the two-dimensional (2-D) NRI TL structure used to demonstrate negative refraction and focusing experimentally at microwave frequencies [6], [7]. Furthermore, a 1-D fast-wave implementation of this metamaterial was shown to exhibit backward-wave radiation from its fundamental spatial harmonic, an effect similar to what Veselago [5] termed "reversed Cherenkov radiation" [8], [9]. This new TL implementation of a NRI metamaterial offers a number of attractive features. It is planar, exhibits large bandwidths of NRI operation and experiences low transmission losses [7].

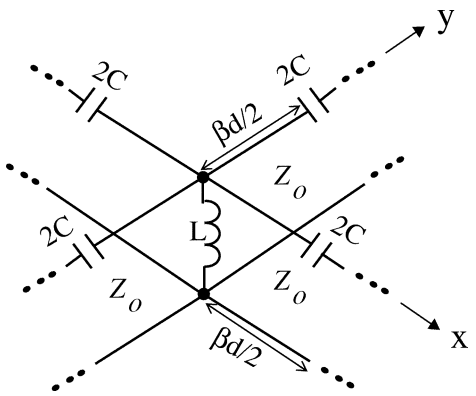

Fig. 1. The unit cell of a 2-D negative refractive index TL structure.

A 1-D theory of operation for the NRI TL metamaterial was presented in [6]–[10] which considered propagation solely along the structure's principal axes. In addition, 2-D numerically obtained (based on the finite element method) dispersion characteristics have been reported in [11]. In this paper, 2-D Bloch theory is utilized to explain the propagation characteristics of the NRI TL structure and to derive useful design equations. Voltage and current relationships, Bloch impedance expressions and dispersion equations are first developed for a generalized 2-D periodic electrical network. These basic relations are then applied to the NRI TL structure. Various passbands and stopbands of the NRI TL structure are presented in the form of a 2-D Brillouin diagram and intuitively explained using the theory developed. Expressions for effective material parameters at frequencies of homogeneous and isotropic NRI operation are also derived, which provide a simplified understanding of the band structure. To verify the analytic expressions derived in this paper, simulation results showing negative refraction are presented. Finally, the proper excitation and termination of finite sized structures is achieved thus eliminating edge effects in the negative refraction results.

II. Theory of Generalized 2-D Periodic Electrical Networks

The propagation characteristics of a generalized periodic structure are examined in this section. Bloch analysis is applied to the generic four port electrical network shown in Fig. 2. The general formulation applies to a wide range of periodic structures including anisotropic [12] and nonreciprocal designs.

Manuscript received September 30, 2002; revised December 10, 2002.

The authors are with The Edward S. Rogers Sr. Department of Electrical and Computer Engineering, University of Toronto, Toronto, ON M5S 3G4, Canada (e-mail: grbica@waves.utoronto.ca).

Digital Object Identifier 10.1109/TAP.2003.817543

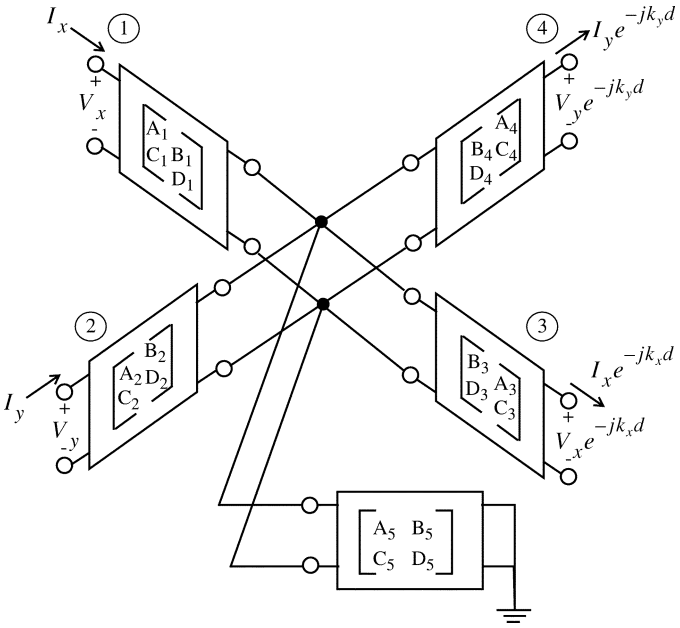

Fig. 2. The unit cell of a general 2-D periodic electrical T-network.

It has been included since it can offer insight into recent electromagnetic bandgap structures [13] and may motivate new TL based metamaterials. This general theory is subsequently applied to the NRI TL structure of Fig. 1 in the following sections. The periodic structure under consideration is general in that the four port networks or unit cells are represented by an arbitrary T-network of transmission matrices as depicted in Fig. 2. As shown, four transmission matrices characterize the four series branches of the T-network while a separate transmission matrix represents the shunt branch. Four different series branches are considered to account for anisotropies that may exist as in the structures of [12]. An infinite periodic structure consisting of a 2-D array of such unit cells can be analyzed by applying Bloch boundary conditions to the voltages and currents at the ports of the unit cell. As depicted in Fig. 2, the voltage and current at one port can be related to those at the opposite port by a wavenumber k_x or k_y in the x and y directions, respectively

$$V_1 = V_x,\ V_3 = V_x e^{-jk_x d},\ I_1 = I_x,\ I_3 = I_x e^{-jk_x d} \quad (1)$$

$$V_2 = V_y,\ V_4 = V_y e^{-jk_y d},\ I_2 = I_y,\ I_4 = I_y e^{-jk_y d} \quad (2)$$

where V_1 to V_4 and I_1 to I_4 represent the voltages and currents at the four ports of the unit cell. Two equations can be obtained by applying Kirchhoff's voltage law (KVL) in the x and y directions. One equation relates V_x to I_x and the other V_y to I_y. Applying KVL from port 3 to port 4 yields a third equation relating V_x, I_x, V_y and I_y. Finally, applying Kirchhoff's current law to the central node of the T-network provides a fourth equation relating V_x, I_x, V_y and I_y. These four equations form the following system of linear homogeneous equations

$$(F)\begin{pmatrix} V_x \\ I_x \\ V_y \\ I_y \end{pmatrix} = \begin{pmatrix} f_{11} & f_{12} & 0 & 0 \\ 0 & 0 & f_{23} & f_{24} \\ f_{31} & f_{32} & f_{33} & f_{34} \\ f_{41} & f_{42} & f_{43} & f_{44} \end{pmatrix} \begin{pmatrix} V_x \\ I_x \\ V_y \\ I_y \end{pmatrix} = \begin{pmatrix} 0 \\ 0 \\ 0 \\ 0 \end{pmatrix} \quad (3)$$

$$\begin{aligned}
f_{11} &= 1 - \left(A_1 - \frac{B_1 C_1}{D_1}\right) D_3 e^{-jk_x d} \\
f_{12} &= -\left(A_1 - \frac{B_1 C_1}{D_1}\right) B_3 e^{-jk_x d} - \frac{B_1}{D_1} \\
f_{23} &= 1 - \left(A_2 - \frac{B_2 C_2}{D_2}\right) D_4 e^{-jk_y d} \\
f_{24} &= -\left(A_2 - \frac{B_2 C_2}{D_2}\right) B_4 e^{-jk_y d} - \frac{B_2}{D_2} \\
f_{31} &= D_3 e^{-jk_x d} \quad f_{32} = B_3 e^{-jk_x d} \\
f_{33} &= -D_4 e^{-jk_y d} \quad f_{34} = -B_4 e^{-jk_y d} \\
f_{41} &= \frac{C_1}{C_1 B_1 - D_1 A_1} - C_3 e^{-jk_x d} - \frac{D_5 D_3}{B_5} e^{-jk_x d} \\
f_{42} &= \frac{-A_1}{C_1 B_1 - D_1 A_1} - A_3 e^{-jk_x d} - \frac{D_5 B_3}{B_5} e^{-jk_x d} \\
f_{43} &= \frac{C_2}{C_2 B_2 - A_2 D_2} - C_4 e^{-jk_y d} \\
f_{44} &= \frac{-A_2}{C_2 B_2 - A_2 D_2} - A_4 e^{-jk_y d}.
\end{aligned} \quad (4)$$

Substituting the first two rows of the coefficient matrix F into the last two rows and assuming the series branches of the T-network are reciprocal yields the following simplified system of linear homogeneous equations [(5) and (6), shown at the bottom of the page]:

$$(G)\begin{pmatrix} V_x \\ V_y \end{pmatrix} = \begin{pmatrix} g_{11} & g_{12} \\ g_{21} & g_{22} \end{pmatrix} \begin{pmatrix} V_x \\ V_y \end{pmatrix} = \begin{pmatrix} 0 \\ 0 \end{pmatrix}. \quad (5)$$

$$\begin{aligned}
g_{11} &= \frac{(B_1 D_3 + B_3 D_1) e^{-jk_x d}}{B_3 e^{-jk_x d} + B_1} \\
g_{12} &= \frac{-(B_2 D_4 + B_4 D_2) e^{-jk_y d}}{B_4 e^{-jk_y d} + B_2} \\
g_{21} &= \frac{1 + e^{-2jk_x d} - e^{-jk_x d}\left(C_1 B_3 + B_1 C_3 + A_1 D_3 + D_1 A_3 + \frac{B_1 D_3 D_5 + D_1 B_3 D_5}{B_5}\right)}{B_3 e^{-jk_x d} + B_1} \\
g_{22} &= \frac{1 + e^{-2jk_y d} - e^{-jk_y d}(C_2 B_4 + B_2 C_4 + A_2 D_4 + D_2 A_4)}{B_2 + B_4 e^{-jk_y d}}.
\end{aligned} \quad (6)$$

For nontrivial solutions, the determinant of the coefficient matrix G must vanish. This yields the following dispersion equation for the periodic structure

$$\begin{aligned}0 =&(B_1D_3 + B_3D_1)[2\cos(k_yd) - (C_2B_4 \\ &+ B_2C_4 + A_2D_4 + D_2A_4)] + (B_2D_4 + B_4D_2) \\ &\times [2\cos(k_xd) - (C_1B_3 + B_1C_3 \\ &+A_1D_3 + D_1A_3 + \frac{B_1D_3D_5}{B_5} + \frac{B_3D_1D_5}{B_5}\Big)\Big]. \quad (7)\end{aligned}$$

The periodic structures analyzed in the following sections mimic isotropic media. As a result, they consist of T-networks with identical series branches and the following simplifications apply

$$\begin{aligned}A =&A_1 = A_2 = A_3 = A_4 \\ B =&B_1 = B_2 = B_3 = B_4 \\ C =&C_1 = C_2 = C_3 = C_4 \\ D =&D_1 = D_2 = D_3 = D_4. \quad (8)\end{aligned}$$

Given (8), the dispersion equation (7) reduces to

$$0 = BD\left[\cos(k_xd) + \cos(k_yd) + 2 - 4AD - BD\frac{D_5}{B_5}\right]. \quad (9)$$

Bloch impedances as in a standard 1-D periodic structure can be defined using the first two rows of matrix F in (3). There are two possible Bloch impedances for power flow in the positive x and y directions, Z_x and Z_y, respectively

$$Z_x = \frac{f_{12}}{f_{11}} = \frac{V_x}{I_x} = \frac{B_1 + B_3e^{-jk_xd}}{D_1 - D_3e^{-k_xd}} \quad (10)$$

$$Z_y = \frac{f_{24}}{f_{23}} = \frac{V_y}{I_y} = \frac{B_2 + B_4e^{-jk_yd}}{D_2 - D_4e^{-k_yd}}. \quad (11)$$

Given (8), the Bloch impedance expressions simplify to

$$Z_x = \frac{V_x}{I_x} = \frac{-jB}{D\tan\left(\frac{k_xd}{2}\right)} \quad (12)$$

$$Z_y = \frac{V_y}{I_y} = \frac{-jB}{D\tan\left(\frac{k_yd}{2}\right)}. \quad (13)$$

Last, the dependence between V_x and V_y can be found for a given direction of propagation defined by k_x and k_y. It can be derived using the first row of matrix G in (5)

$$V_x = V_y\frac{g_{12}}{g_{11}} = V_y\left[\frac{B_2D_4 + B_4D_2}{B_4 + B_2e^{jk_yd}}\right]\left[\frac{B_3 + B_1e^{jk_xd}}{B_1D_3 + B_3D_1}\right]. \quad (14)$$

Under the assumption that the series branches consist of identical networks, (14) reduces to

$$V_x = V_y\frac{1 + e^{jk_xd}}{1 + e^{jk_yd}}. \quad (15)$$

Equation (1) defines the relationship between the voltages and currents at ports 1 and 3, while (2) specifies the relationship between the voltages and currents at ports 2 and 4. The Bloch impedances [(10)–(13)], on the other hand, define the dependence between the voltage and current at the same port. Equations (14) and (15) complete the picture by specifying the dependence between the voltages at ports 1 and 3. As a result, all four port voltages and currents can now be related given k_x and k_y.

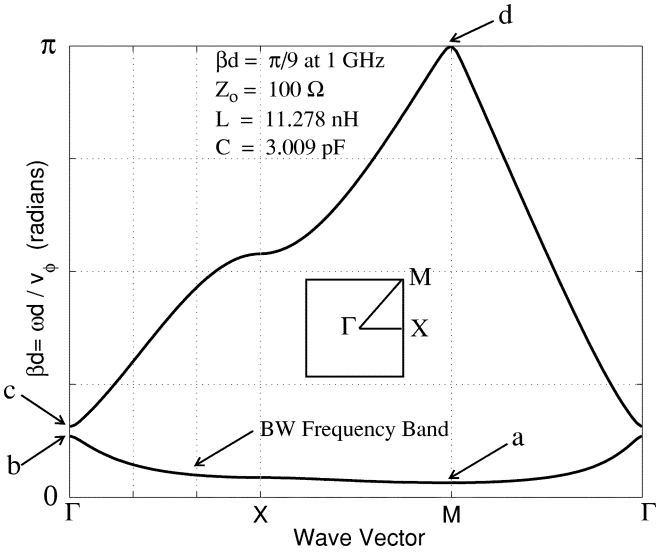

Fig. 3. Typical dispersion characteristic of a NRI TL structure.

III. Negative Refractive Index *L*-*C* Networks

At this point, the propagation characteristics of the NRI TL shown in Fig. 1 are investigated. The expressions derived in the previous section for a periodic structure composed of general T-networks are applied to this specific structure. The NRI TL structure has identical reciprocal series branches which can be represented by the transmission matrix of a 2C capacitor connected in series with a $\beta d/2$ section of TL

$$\begin{pmatrix} A & B \\ C & D \end{pmatrix} = \begin{pmatrix} \cos\left(\frac{\beta d}{2}\right) + \frac{1}{2Z_o2\omega C}\sin\left(\frac{\beta d}{2}\right) & jZ_o\sin\left(\frac{\beta d}{2}\right) - \frac{j}{2\omega C}\cos\left(\frac{\beta d}{2}\right) \\ \frac{j}{2Z_o}\sin\left(\frac{\beta d}{2}\right) & \cos\left(\frac{\beta d}{2}\right) \end{pmatrix} \quad (16)$$

where Z_o is the characteristic impedance, β is the propagation constant, and d is the length of the interconnecting TL sections. The shunt branch is defined by the following transmission matrix

$$\begin{pmatrix} A_5 & B_5 \\ C_5 & D_5 \end{pmatrix} = \begin{pmatrix} 1 & j\omega L \\ 0 & 1 \end{pmatrix}. \quad (17)$$

Substituting (16) and (17) into the dispersion equation (9) yields

$$\begin{aligned}\sin^2\left(\frac{k_xd}{2}\right) + \sin^2\left(\frac{k_yd}{2}\right) = \frac{1}{2}\Bigg[2\sin\left(\frac{\beta d}{2}\right) \\ -\frac{1}{Z_o\omega C}\cos\left(\frac{\beta d}{2}\right)\Bigg]\left[2\sin\left(\frac{\beta d}{2}\right) - \frac{Z_o}{2\omega L}\cos\left(\frac{\beta d}{2}\right)\right] \quad (18)\end{aligned}$$

where $\beta = \omega/v_\phi$ and v_ϕ is the phase velocity of the interconnecting TL.

Dispersion equation (18) defines the band structure of the NRI TL metamaterial. A representative dispersion characteristic is plotted in Fig. 3 in the form of a Brillouin diagram. An intuitive understanding of the band structure is gained by examining various resonances which identify the location and nature

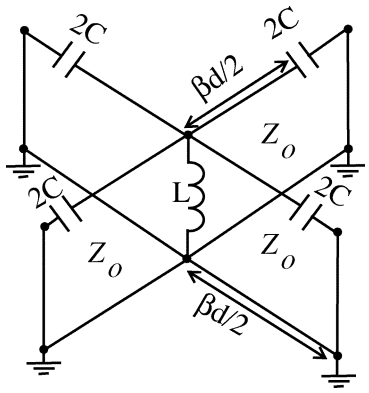

Fig. 4. Resonance identifying the onset of the initial passband.

of the structure's passbands and stopbands. It is clear from the high-pass configuration of the NRI TL structure that a stopband exists for low frequencies of operation. As the frequency is increased, the unit cells begin to resonate marking the onset of the structure's first passband of operation. The frequency at which the first passband begins (point (a) in Fig. 3) can be computed by setting $k_x d = k_y d = \pi$ in dispersion equation (18). Rearranging the dispersion equation yields the following expression

$$0 = \cos\left(\frac{\beta d}{2}\right)\left[\left(4 - \frac{1}{2\omega^2 LC}\right)\cos\left(\frac{\beta d}{2}\right) + 2\sin\left(\frac{\beta d}{2}\right)\left(\frac{1}{Z_o \omega C} + \frac{Z_o}{2\omega L}\right)\right]. \quad (19)$$

The start of the passband (a) is found by setting the second product term in (19) equal to zero. Setting the term to zero is equivalent to computing the resonant frequency ω_1 of the unit cell with all four terminals short circuited to ground as shown in Fig. 4. A resonance occurs between the four parallel sections of $\beta d/2$ transmission lines grounded by $2\mathrm{C}$ capacitors, and the loading inductor L

$$\frac{Z_o\left(\frac{-1}{\omega_1 2C} + Z_o \tan\left(\frac{\beta_1 d}{2}\right)\right)}{4\left(Z_o + \frac{\tan\left(\frac{\beta_1 d}{2}\right)}{\omega_1 2C}\right)} = -\omega_1 L \quad (20)$$

where $\beta_1 = \omega_1/v_\phi$. Within this first passband of operation [between points (a) and (b)], the structure supports backward-wave propagation since the wave vector $[k_x, k_y]$ and direction of power flow (given by the gradient to the dispersion surface of the BW passband) are antiparallel. A more intuitive explanation as to why this band supports backward wave propagation is offered in the following section. As the frequency is increased within the backward-wave passband, the magnitude of the wavenumbers decreases from $k_x = k_y = \pi/d$ at the initial resonance (a) to $k_x = k_y = 0$ at point (b). At point (b) the NRI TL structure enters its second stopband region which extends to point (c). The frequencies ω_2 and ω_3 of the stopband edges (points (b) and (c) in Fig. 3) can be solved for by setting $k_x d = k_y d = 0$ in the dispersion relation. The stopband edge ω_2 is defined by setting the first term of (18) to zero

$$\frac{1}{\omega_2(2C)} = Z_o \tan\frac{\beta_2 d}{2} \quad (21)$$

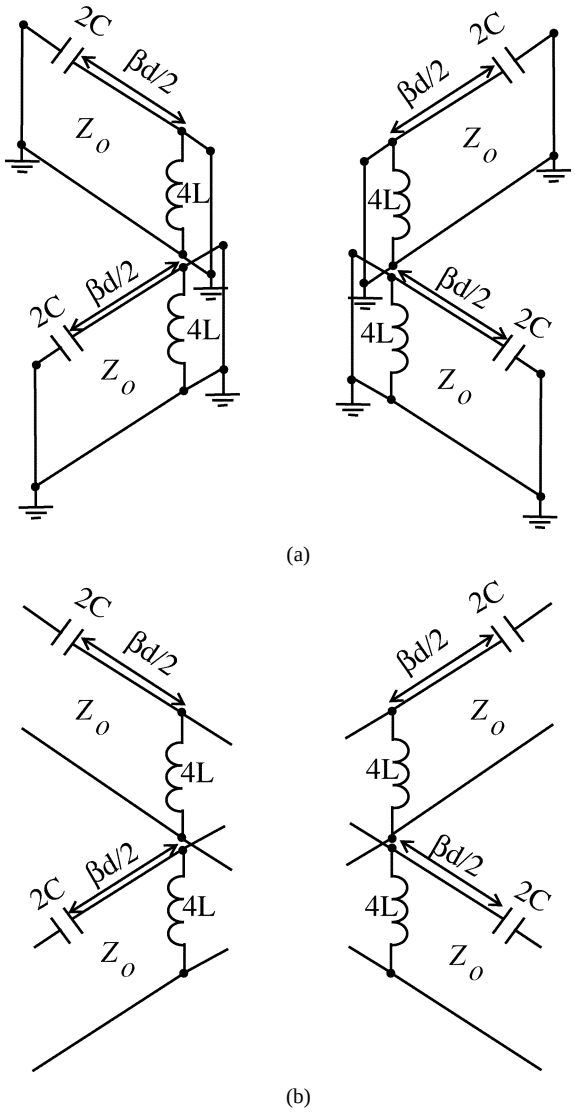

Fig. 5. Resonances identifying the edges of the second stopband.

where $\beta_2 = \omega_2/v_\phi$. The frequency ω_2 represents either point (b) or (c) depending on the relative values of L and C in the NRI TL structure. Equation (21) indicates that at ω_2, the resonance shown in Fig. 5(a) occurs. The ports and central node of the unit cell act as if they are shorted to ground, thereby short circuiting the shunt inductors. At this resonance, each $\beta d/2$ short-circuited TL section resonates with a $2\mathrm{C}$ capacitor.

The other stopband edge ω_3 [either point (b) or (c)] can be solved for by setting the second term in (18) equal to zero

$$\frac{1}{\omega_3(4L)} = Y_o \tan\left(\frac{\beta_3 d}{2}\right) \quad (22)$$

where Y_o is the characteristic admittance of interconnecting TL sections $(1/Z_o)$ and $\beta_3 = \omega_3/v_\phi$. This expression suggests that the resonance depicted in Fig. 5(b) occurs at ω_3. The central node and ports of the unit cell act as if they are open circuited thereby open circuiting the series capacitors. Accordingly, each open circuited $\beta d/2$ section of TL resonates with a $4\mathrm{L}$ inductor.

Beyond the second stopband, there exists another passband supporting forward-wave propagation that extends from points

(c) to (d). Its upper cutoff frequency ω_4 (labeled (d) in Fig. 3) can be found by setting the first term in (19) equal to zero

$$\cos\left(\frac{\beta_4 d}{2}\right) = 0 \tag{23}$$

where $\beta_4 = \omega_4/v_\phi$. This occurs when the interconnecting TL sections become a half wavelength. It is important to note that as the electrical length of the interconnecting TLs vanishes, the stopband edges ω_1, ω_2 and ω_3 are pushed to infinity. As a result, large bandwidths of NRI operation are achievable with such TL structures.This was confirmed by the experimental focusing results of [7], which reported a NRI within an octave bandwidth.

Using (12) and (13), the Bloch impedances in the x and y directions for the NRI TL metamaterial are found to be

$$Z_x = \frac{Z_o \tan\left(\frac{\beta d}{2}\right) - \frac{1}{2\omega C}}{\tan\left(\frac{k_x d}{2}\right)},\ Z_y = \frac{Z_o \tan\left(\frac{\beta d}{2}\right) - \frac{1}{2\omega C}}{\tan\left(\frac{k_y d}{2}\right)}. \tag{24}$$

The unit cells of the NRI TL metamaterial are symmetrical, therefore the Bloch impedances looking into the positive and negative x and y directions are identical.

IV. The NRI TL Structure as an Effective Medium: The Homogeneous Limit

For a given frequency range within the backward-wave passband, the NRI TL structure shown in Fig. 1 appears isotropic and homogeneous. It can, therefore, be considered an effective medium. As a result, effective material parameters such as permittivity and permeability can be assigned to the periodic structure. This effective medium perspective provides additional insight and a simplified understanding of the NRI TL structure's propagation characteristics.

The frequency range where the NRI TL structure acts as an effective medium occurs when the interconnecting TL sections are electrically short ($\beta d \ll 1$) and the per-unit-cell phase delays are small ($k_x d \ll 1, k_y d \ll 1$). Under these two conditions, the dispersion equation (18) simplifies to

$$k_x^2 + k_y^2 = \left(\beta - \frac{1}{Z_o \omega C d}\right)\left(2\beta - \frac{Z_o}{\omega L d}\right). \tag{25}$$

Letting $k_x = k\cos\phi$ and $k_y = k\sin\phi$ (where ϕ is an angle with the x axis), $\epsilon =$ twice the per unit length capacitance of the interconnecting TLs and $\mu =$ the per unit length inductance of the interconnecting TLs, the dispersion equation takes the form

$$k^2 = \omega^2 \mu_e \epsilon_e \text{ where } \mu_e = \left(\mu - \frac{1}{\omega^2 C d}\right),\ \epsilon_e = \left(\epsilon - \frac{1}{\omega^2 L d}\right). \tag{26}$$

The variables ϵ and μ are related to the permittivity and permeability of the unloaded 2-D TL mesh shown in Fig. 6, which acts as the host medium. On the other hand, μ_e represents the effective permeability and ϵ_e the effective permittivity of the NRI TL structure. Dispersion equation (26) confirms that the metamaterial appears isotropic and homogeneous when βd, $k_x d$ and $k_y d$ are small quantities. It also indicates that the loading series capacitor provides a negative magnetic susceptibility since it reduces the effective permeability of the host medium. The loading shunt inductance, however, provides a negative electric susceptibility since it reduces the host medium's permittivity.

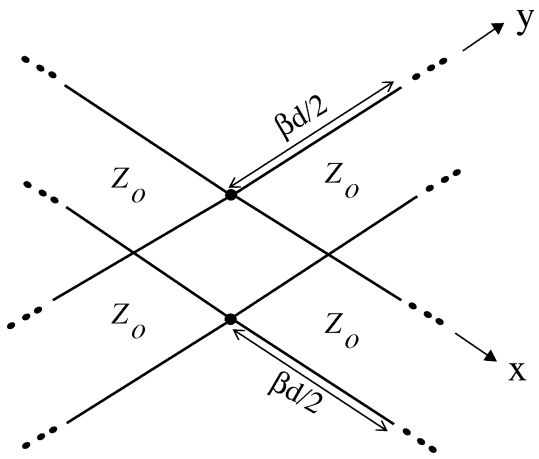

Fig. 6. 2-D TL mesh.

Within the backward-wave propagation band, the negative electric and negative magnetic susceptibilities overcome the permittivity and permeability (ϵ, μ) of the host medium and the effective material parameters (ϵ_e, μ_e) become negative. Therefore, the structure acts as a NRI medium at these frequencies. The negative material parameters intuitively explain the backward-wave nature of the propagation within the first passband of operation. The dispersion equation (26) also suggests that at high frequencies the effective material parameters become positive due to a decrease of the electric and magnetic susceptibilities. The positive material parameters give rise to a high frequency passband supporting forward-wave propagation. This propagation band corresponds to the passband in Fig. 3 that extends from (c) to (d). At frequencies between the backward-wave and forward-wave propagation bands one of the effective material parameters (ϵ_e or μ_e) is positive while the other is negative. As a result, the wavenumber k becomes imaginary indicating the existence of a stopband. This corresponds to the stopband stretching from point (b) to (c) in Fig. 3.

For frequency bands where there is nearly isotropic propagation, the Bloch impedances expressions reduce to

$$Z_x = \frac{Z_B}{\cos\phi},\ Z_y = \frac{Z_B}{\sin\phi} \text{ where } Z_B = \sqrt{\frac{\mu_e}{\epsilon_e}}. \tag{27}$$

These impedance expressions are of the same form as the wave impedances of a vertically polarized electromagnetic plane wave propagating along the horizontal plane of a homogeneous and isotropic medium.

V. Investigation of Negative Refraction

In the following section, dispersion equations and Bloch impedance expressions are utilized to design two media with effective material parameters (ϵ_e, μ_e) that are equal in magnitude but opposite in sign, thus leading to a relative refractive index of $n = -1$. This implies that the Bloch impedances for both media are identical while their wave vectors $[k_x, k_y]$ are antiparallel for a given direction of power flow. Simulated results of negative refraction between these two media are

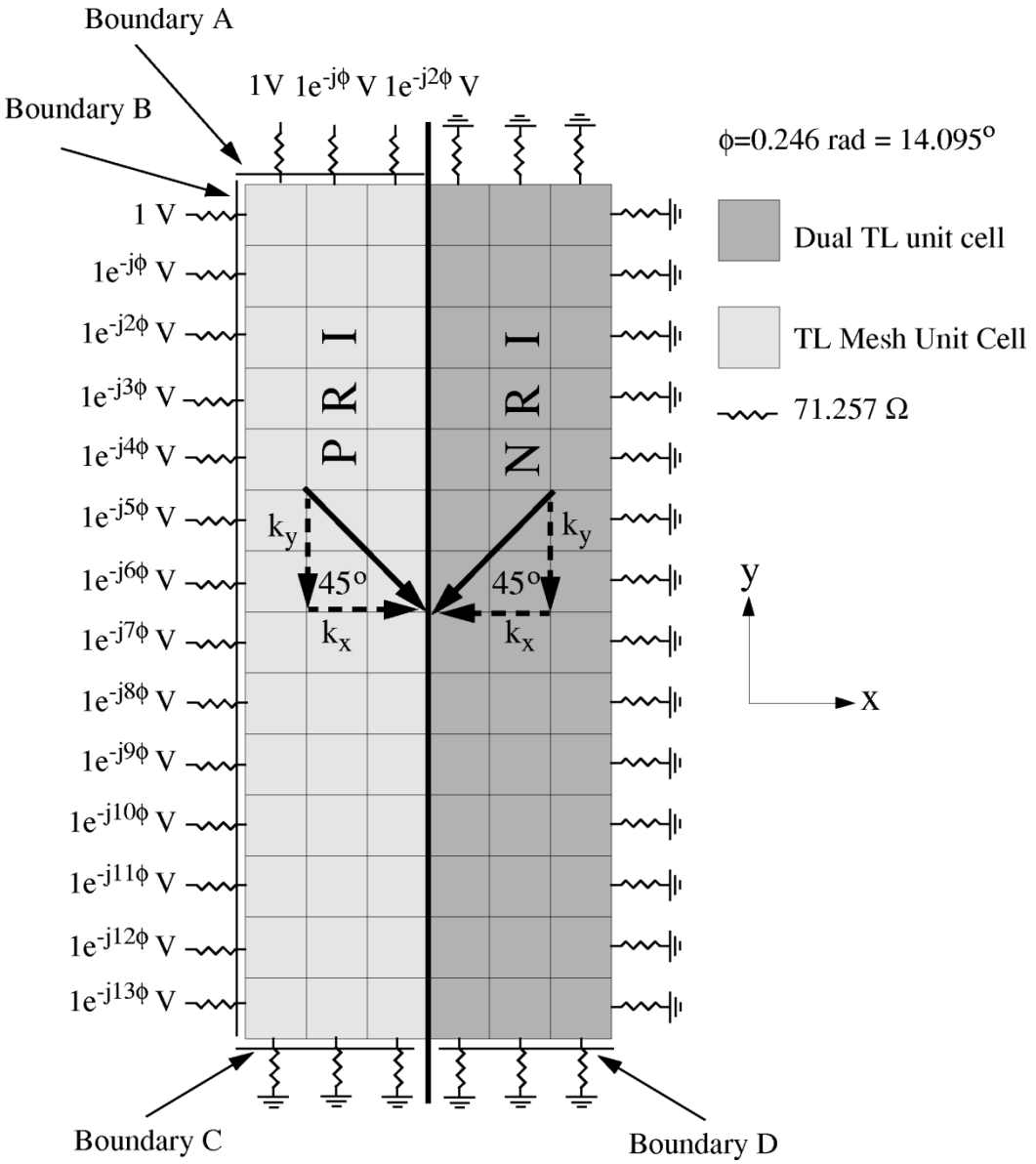

Fig. 7. Negative refraction simulation set up corresponding to a relative refractive index $n = -1$.

presented and the issue of properly exciting and terminating such structures is addressed.

A medium with positive material parameters will be referred to as a PRI (positive refractive index) medium just as a medium with negative material parameters was designated a NRI metamaterial. The NRI metamaterial is implemented as the TL structure shown in Fig. 1 and the PRI material is realized by a 2-D mesh of TLs. A unit cell of the PRI is shown in Fig. 6. The frequency of operation is chosen to be 1 GHz. At this frequency, Z_x is set to 50 Ω for x-directed plane waves ($k_y = 0$) in both media. The phase delay per-unit-cell for x-directed waves is fixed to $k_x d = \pi/9$ in the PRI material and $k_x d = -\pi/9$ in the NRI metamaterial (see Fig. 7).

In the NRI metamaterial, the interconnecting TLs are assigned a characteristic impedance of 100 Ω and their phase delay is set to $\beta d = \pi/9$ radians. A small phase delay (βd) is chosen to ensure near isotropic propagation. Specifying $Z_o = 100\ \Omega$, $\beta d = \pi/9$, $Z_x = 50\ \Omega$, $k_x d = -\pi/9$ and $k_y d = 0$ in (18) and (24) yields the following values for the NRI TL structure's loading inductor and capacitor

$$C = 3.009\ \text{pF},\ L = 11.278\ \text{nH}. \tag{28}$$

To design the PRI material, a dispersion equation and Bloch impedance expressions for the TL mesh structure shown in Fig. 6 are required. The dispersion equation for the TL mesh can be derived using (9). It is given by the following expression:

$$\sin^2\left(\frac{k_x d}{2}\right) + \sin^2\left(\frac{k_y d}{2}\right) = 2\sin^2\left(\frac{\beta d}{2}\right). \tag{29}$$

Utilizing (12) and (13), the Bloch impedance in the x and y directions for the TL mesh can also be found

$$Z_x = Z_o \frac{\tan\left(\frac{\beta d}{2}\right)}{\tan\left(\frac{k_x d}{2}\right)},\ Z_y = Z_o \frac{\tan\left(\frac{\beta d}{2}\right)}{\tan\left(\frac{k_y d}{2}\right)}. \tag{30}$$

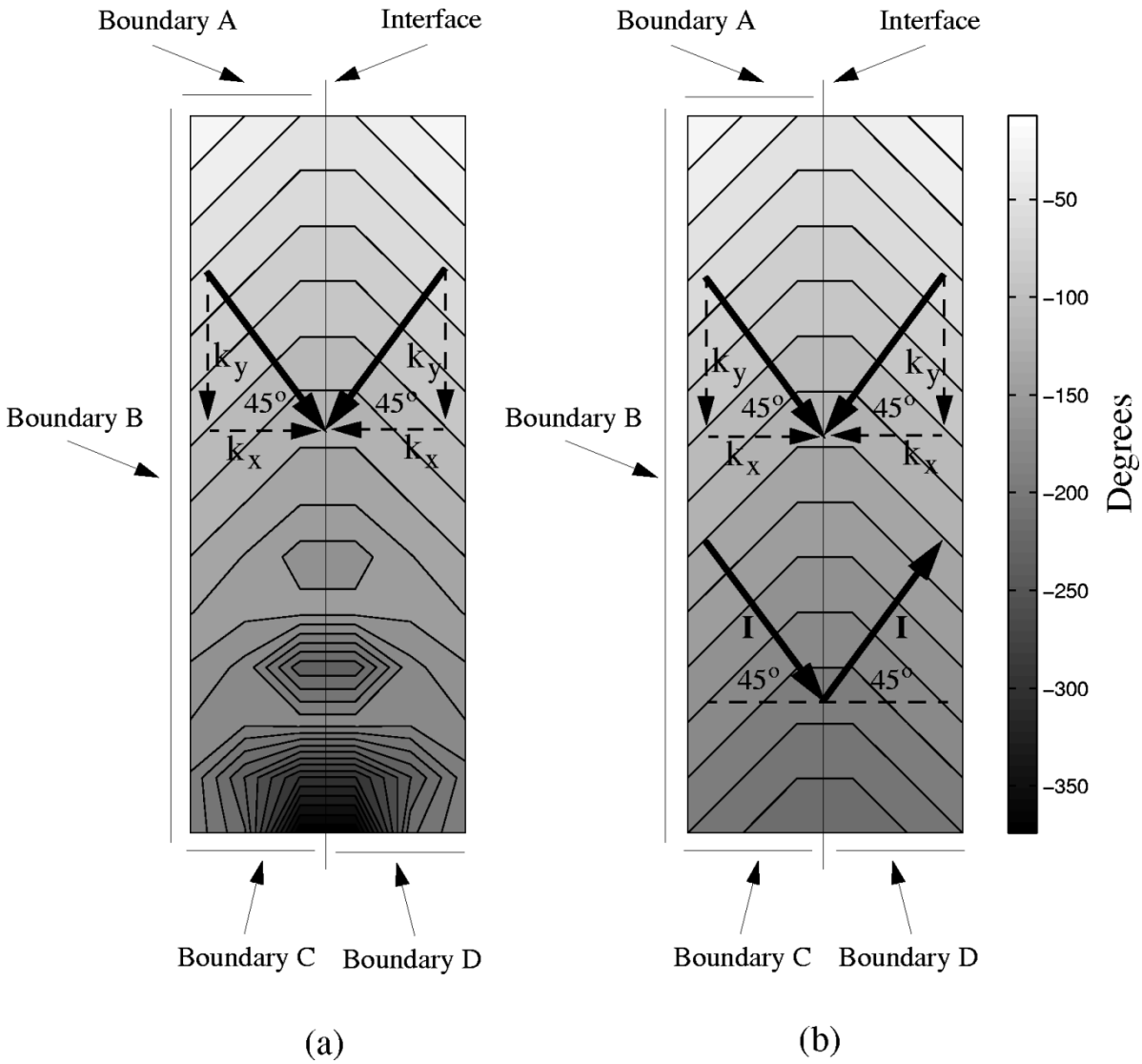

Fig. 8. Simulated voltage phase progression demonstrating negative refraction.

Recalling that $Z_x = 50\ \Omega$, $k_x d = -\pi/9$ when $k_y d = 0$ for the TL mesh and solving (29) and (30) results in the following characteristic impedance (Z_o) and propagation constant (β) of the TLs in the TL mesh

$$\beta d = 0.246 \text{ rad} = 14.095^\circ,\ Z_o = 71.257\ \Omega. \qquad (31)$$

The PRI and NRI structures were designed considering propagation solely along the x axis. This was sufficient since both media exhibit homogeneous and isotropic propagation characteristics at 1 GHz. Homogeneous propagation characteristics were accomplished by maintaining $k_x d \ll 1$, $k_y \ll 1$ and $\beta d \ll 1$ for both PRI and NRI structures.

Refraction at the interface between the PRI and NRI structures was explored using Agilent's Advanced Design System (ADS) circuit simulator. The PRI and NRI structures simulated extend 3 cells in the x direction and 14 cells in the y direction as illustrated in Fig. 7. A plane wave incident from the PRI structure was modeled using an array of linearly phase-tapered voltage generators along boundaries A and B as depicted in Fig. 7. For convenience, a 45° angle of incidence was chosen. At this angle of incidence, the per-unit-cell phase delays are equal ($k_x d = k_y d$) and can be found to be 0.246 *rad* using (29). Moreover, (15) specifies that $V_x = V_y$ since $k_x = k_y$. For this reason, the voltage generators at the upper left corner cell were set to the same voltage, 1 V. A progressive phase delay of 0.246 radians (14.095°) between the remaining voltage generators was established as shown in Fig. 7. All the generators and boundaries of the simulated structure were terminated in 71.257 Ω resistors. This termination resistance corresponds to Z_x and Z_y for a 45° angle of incidence and, therefore, matches all boundaries of the PRI and NRI structures to their common Bloch impedance. A contour plot of the voltage phases at the central nodes of each cell is shown in Fig. 8(a). As expected, the voltage waves undergo negative refraction corresponding to $n = -1$ as they pass from the NRI to the PRI material. Nevertheless, the phase plot of Fig. 8(a) exhibits distinct phase errors near boundaries C and D. The phase errors occur due to the resistive termination of the waves incident on boundary C. These waves never reach the interface. In an infinite medium these waves would eventually hit the interface, refract and re-enter boundary D. In order to model an infinite medium, voltage generators were placed along boundary D to recover these terminated waves. As can be seen

from the phase plot in Fig. 8(b), the phase fronts undergo perfect negative refraction thereby verifying the design equations and confirming that both PRI and NRI media are correctly designed and properly terminated. Furthermore, the current (I) exhibits the same phase progression as the voltage waves but also undergoes a change in direction as shown in Fig. 8(b), indicating that the power of the incident plane wave is also negatively refracted. Due to the 2-D Bloch analysis that was employed in designing and properly terminating the PRI and NRI structures, the edge effects evident in previously reported results of negative refraction [6] have been eliminated.

VI. Conclusion

In this paper, Bloch analysis was applied to a generalized 2-D periodic electrical network. The results were then used to explain the propagation characteristics of the NRI TL metamaterial. A 2-D Brillouin diagram for the metamaterial was presented and the band structure intuitively explained. Voltage and current relations as well as dispersion equations which aid in the design of such structures were shown. Additionally, the effective material parameters of the metamaterial were derived for frequency ranges of isotropic and homogeneous operation. Simulation results of negative refraction were presented showing that two separate media of relative index $n = -1$ can be devised using the derived design equations. Proper termination and excitation of finite size structures was achieved thus eliminating edge effects in the simulations. The developed theory can be utilized to accurately design NRI TL metamaterials for applications such as compact lens antennas, low cost beam steered antennas and antenna multiplexers.

References

[1] D. R. Smith, W. J. Padilla, D. C. Vier, S. C. Nemat-Nasser, and S. Schultz, "Composite medium with simultaneously negative permeability and permittivity," *Phys. Rev. Lett.*, vol. 84, pp. 4184–4187, May 2000.

[2] J. B. Pendry, "Negative refraction makes a perfect lens," *Phys. Rev. Lett.*, vol. 85, pp. 3966–3969, Oct. 2000.

[3] D. R. Smith and N. Kroll, "Negative refractive index in left-handed materials," *Phys. Rev. Lett.*, vol. 85, pp. 2933–2936, Oct 2000.

[4] R. A. Shelby, D. R. Smith, and S. Schultz, "Experimental verification of a negative index of refraction," *Science*, vol. 292, pp. 77–79, Apr. 2001.

[5] V. G. Veselago, "The electrodynamics of substances with simultaneously negative values of ϵ and μ," *Sov. Phys. Usp.*, vol. 10, pp. 509–514, Jan.-Feb. 1968.

[6] A. K. Iyer and G. V. Eleftheriades, "Negative refractive index metamaterials supporting 2-D wave propagation," *IEEE MTT-S Int. Microwave Symp. Dig.*, vol. 2, pp. 1067–1070, June 2002.

[7] G. V. Eleftheriades, A. K. Iyer, and P. C. Kremer, "Planar negative refractive index media using periodically L-C loaded transmission lines," *IEEE Trans. Microwave Theory Tech.*, vol. 50, pp. 2702–2712, Dec. 2002.

[8] A. Grbic and G. V. Eleftheriades, "A backward-wave antenna based on negative refractive index L-C networks," in *IEEE Int. Symp. Antennas Propagat.*, vol. 4, San Antonio, TX, June 16–21, 2002, pp. 340–343.

[9] ——, "Experimental verification of backward-wave radiation from a negative refractive index metamaterial," *J. Appl. Phys.*, vol. 92, pp. 5930–5935, Nov. 2002.

[10] G. V. Eleftheriades, O. Siddiqui, and A. K. Iyer, "Transmission line models for negative refractive index media and associated implementations," IEEE Microwave Wireless Components Lett., Aug. 2002, to be published.

[11] A. Grbic and G. V. Eleftheriades, "Dispersion analysis of a microstrip (based negative refractive index periodic structure," IEEE Microwave Wireless Compon. Lett., Sept. 2002, to be published.

[12] K. G. Balmain, A. E. Luttgen, and P. C. Kremer, "Resonance cone formation, reflection, refraction and focusing in a planar, anisotropic metamaterial," IEEE Antennas Wireless Propagat. Lett., Oct. 2002, to be published.

[13] D. Sievenpiper, L. Zhang, R. F. J. Broas, N. G. Alexopolous, and E. Yablonovitch, "High impedance electromagnetic surfaces with a forbidden frequency band," *IEEE Trans. Microwave Theory Tech.*, vol. 47, pp. 2059–2074, Nov. 1999.

Anthony Grbic (S'00) received the B.A.Sc. and M.A.Sc. degrees in electrical engineering from the University of Toronto, Toronto, ON, Canada, in 1998 and 2001, respectively, where he is currently working toward the Ph.D. degree.

His research interests include planar millimeter-wave antennas, circuits, negative refractive index metamaterials, and periodic structures.

Mr. Grbic received the Best Student Paper Award, at the 2000 Antenna Technology and Applied Electromagnetics Symposium.

George V. Eleftheriades (S'86–M'88–SM'02) received the Ph.D. and M.S.E.E. degrees in electrical engineering from the University of Michigan, Ann Arbor, in 1993 and 1989, respectively. He received the diploma (with distinction) in electrical engineering from the National Technical University of Athens, Greece, in 1988.

During 1994–1997, he was with the Swiss Federal Institute of Technology, Lausanne, Switzerland, where he was engaged in the design of millimeter and submillimeter-wave receivers and in the creation of fast CAD tools for planar packaged microwave circuits. Currently, he is an Associate Professor with the Department of Electrical and Computer Engineering, University of Toronto, Toronto, ON, Canada. He has authored or coauthored more than 80 articles in refereed journals and conference proceedings. His current research interests include negative refractive index metamaterials, IC antennas and components for broadband wireless communications, novel beam-steering techniques, low-loss silicon micromachined components, millimeter-wave radiometric receivers, and electromagnetic design for high-speed digital circuits.

Dr. Eleftheriades was a corecipient of the Best Paper Award at the 6th International Symposium on Antennas (JINA), France 1990 and the Ontario Premier's Research Excellence Award in 2001. His graduate students won Student Paper Awards in the 2000 Antenna Technology and Applied Electromagnetics Symposium, the 2002 IEEE International Microwave Symposium, and the 2002 IEEE International Symposium on Antennas and Propagation.